Journal of
Materials Chemistry C

COMMUNICATION

View Article Online
View Journal | View Issue

Cite this: J. Mater. Chem. C, 2016, 4, 10625

Received 27th September 2016,
Accepted 21st October 2016

DOI: 10.1039/c6tc04213a

www.rsc.org/MaterialsC

Ultrasound synthesis of lead halide perovskite nanocrystals†

Dong Myung Jang,[a] Duk Hwan Kim,[a] Kidong Park,[a] Jeunghee Park,*[a] Jong Woon Lee[b] and Jae Kyu Song[b]

We report the ultrasound-induced synthesis of $APbX_3$ perovskite nanocrystals with a wide range of compositions, where A = CH_3NH_3, Cs, or HN=$CHNH_3$ (formamidinium), and X = Cl, Br, or I. Ultrasonic irradiation accelerates dissolution of the precursors (AX and PbX_2) in toluene, and the dissolution rate determines the growth rate of the nanocrystals. We fabricated high-sensitivity photodetectors by homogenously spin coating the uniform size nanocrystals on large-area silicon oxide substrates.

Lead halide perovskites ($APbX_3$, where A is an organic or inorganic cation, and X is a halogen anion) have recently attracted worldwide attention because they exhibit superior solar-power-conversion efficiencies of over 20%.[1] They have unique optical and electrical properties that also make them promising materials for various optoelectronic devices;[2] these properties include direct band gaps, large absorption coefficients, high carrier mobilities, small exciton binding energies, and long charge-diffusion lengths.[3–8] $APbX_3$ perovskite materials are usually synthesized as polycrystalline thin films by the one-step or two-step spin coating method, using PbX_2 and AX precursors that are dissolved in solvents.[9–11]

The synthesis of colloidal perovskite nanocrystals (NCs) has emerged as an important research topic from both fundamental and technological points of view.[12–26] By applying the deposition methods that have been used for quantum dots (*e.g.*, CdSe), such as spin coating, inkjet printing, and mist coating, homogeneous and reproducible thin films of colloidal NCs can be obtained.[27] Perovskite NCs have already demonstrated remarkable potential to become a new class of photoactive materials in future quantum-dot light-emitting diodes (LEDs), solar cells, lasers, and photodetectors.[16,21–26] Ling *et al.* reported that LEDs made of highly emissive $CH_3NH_3PbBr_3$ NCs exhibited higher performances than LEDs prepared from polycrystalline films.[22] Recently, Cha *et al.* reported that interfacial modification of perovskite NCs enhances solar cell efficiency.[23] A sufficiently large optical gains have also been observed in perovskite NCs with low lasing thresholds and high quality factors.[24,25] High-sensitivity photodetectors were fabricated using $CH_3NH_3PbX_3$ and $CsPbX_3$ NCs.[16,26] Nevertheless, simple routes for synthesizing well-defined colloidal perovskite NCs remain highly desirable.

In the present work, we report a new method—ultrasonic irradiation of precursor solutions—for synthesizing $APbX_3$ perovskite NCs, where A = CH_3NH_3 (methylammonium, MA), Cs, or HN=$CHNH_3$ (formamidinium, FA), and X = Cl, Br, or I. Furthermore, mixing MAX (X = Cl, Br or I) and PbX_2 with different halides produced a series of mixed halides with the formulae $APbBr_{3-x}Cl_x$ and $MAPbBr_{3-x}I_x$. Perovskite NCs with various compositions were prepared so that the band gap could be successfully tuned over a wide range. To the best of our knowledge, this is the first report on ultrasound-assisted synthesis of colloidal perovskite NCs. Photodetector devices that exhibited outstanding photosensitivities were fabricated by spin coating the perovskite NCs on thermally oxidized silicon wafers.

The detailed experimental procedure is described in the ESI.† The synthesis and characterization procedures are summarized as follows: AX (=MAX, CsX, or FAX), PbX_2, and OAm were mixed at a molar ratio of 1 : 1 : 3 in toluene; the mixture was sonicated using a probe-type ultrasonicator for 10 min to 3 h. The X-ray diffraction (XRD) patterns of the products showed single perovskite phases with a high degree of purity (ESI,† Fig. S1).

Fig. 1a shows high-resolution transmission electron microscopy (HRTEM) images of rectangular plate-type $CsPbBr_3$ NCs with an average side length of 10 nm. The thickness was estimated to be less than 5 nm. Fig. 1b and c show the lattice-resolved TEM and fast-Fourier-transform (FFT) images of $CsPbBr_3$ and $FAPbBr_3$ NCs, respectively, showing that the edges of the plates were parallel to the [100] direction. The *d*-spacings of the (200) planes were 2.9 and 3.0 Å, consistent with those of cubic-phase $CsPbBr_3$ (a = 5.874 Å) and $FAPbBr_3$ (a = 6.00 Å), respectively.[18,28]

[a] Department of Chemistry, Korea University, Jochiwon 339-700, Korea. E-mail: parkjh@korea.ac.kr
[b] Department of Chemistry, Kyung Hee University, Seoul 130-701, Korea

† Electronic supplementary information (ESI) available. See DOI: 10.1039/c6tc04213a

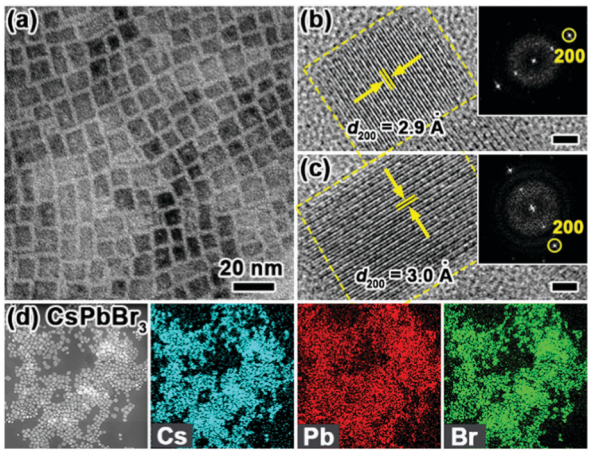

Fig. 1 (a) HRTEM image of monodisperse 10 nm $CsPbBr_3$ NCs. Lattice-resolved and FFT images (scale bar = 2 nm) of cubic-phase (b) $CsPbBr_3$ and (c) $FAPbBr_3$ NCs, showing d_{200} = 2.9 and 3.0 Å, respectively. (d) HAADF STEM images and EDX mappings showing homogeneous distributions of Cs, Pb, and Br in $CsPbBr_3$ NCs.

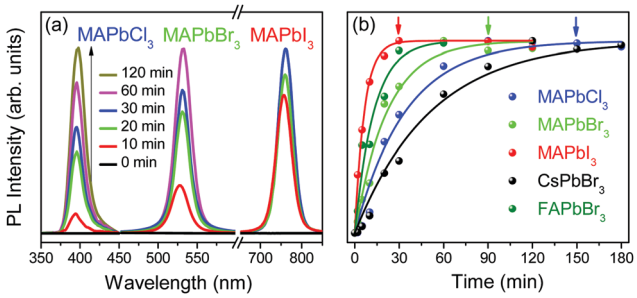

Fig. 2 (a) PL spectra of $MAPbCl_3$, $MAPbBr_3$, and $MAPbI_3$ as functions of time (min), monitored during the sonication of their precursor solutions. (b) PL peak intensity *versus* sonication time for $MAPbCl_3$, $MAPbBr_3$, $MAPbI_3$, $CsPbBr_3$, and $FAPbBr_3$.

Fig. 1d shows the high-angle annular dark field (HAADF) STEM images and EDX mappings of $CsPbBr_3$ NCs. The composition was calculated using the Cs L-shell, Pb L-shell, and Br K-shell. A homogeneous composition, with Cs : Pb : Br = 1 : 1 : 3 (atomic ratio), was found over the entire $CsPbBr_3$ NCs. Perovskite NCs with different compositions also exhibited the same size and morphology (see TEM images and EDX data shown in the ESI,† Fig. S2 and S3).

Since the ultrasonic method is a simple, efficient, low-cost, and environmentally friendly approach, it has been used for the synthesis of various nanostructured materials.[29] The physical phenomenon associated with ultrasound synthesis is cavitation, and acoustic cavitation offers extreme conditions in liquid–solid slurries, with hot spots inside the bubbles (temperatures above 5000 K and pressures exceeding 1000 bar). Recently, Kesari and Athawale used ultrasound to synthesize $MAPbI_3$ nanowires in isopropyl alcohol.[30] Gedanken and coworkers also reported the sonochemical synthesis of $MAPbI_3$ nanocrystals in isopropyl alcohol.[31] The selection of toluene and an organic ligand (OAm) was key to our successful synthesis of NCs with uniform sizes, and is the most distinctive difference from previous sonochemical works. The transient and localized hot spots can promote dissolution of precursors (PbX_2 and AX), supersaturation, and subsequent nucleation and crystallization of perovskite NCs.

In order to understand the role of ultrasonics in the synthesis of perovskite NCs, the relative growth rate was estimated by measuring the photoluminescence (PL) spectra of NCs prepared over different sonication times. Fig. 2a shows the evolution of the PL spectra during sonication of precursor solutions of $MAPbCl_3$, $MAPbBr_3$, and $MAPbI_3$. The excitation light source was a continuous-wave He–Cd laser (wavelength: 325 nm). In Fig. 2b, the PL peak intensity is plotted as a function of the sonication time, and it can be seen that it increased over time until a saturation point was reached. These saturation plateaus (normalized and marked by the arrows) appeared after 150 min ($MAPbCl_3$), 90 min ($MAPbBr_3$), and 30 min ($MAPbI_3$). The results show that the growth rates of $MAPbI_3$ and $MAPbCl_3$ were about 3 times faster and 1.7 times slower than that of $MAPbBr_3$, respectively. The PL spectra of $CsPbBr_3$ and $FAPbBr_3$ show that saturation occurred after 180 and 60 min, respectively, indicating that $CsPbBr_3$ and $FAPbBr_3$ were produced 2 times slower and 1.5 times faster than $MAPbBr_3$, respectively. Photographs (ESI,† Fig. S4) were obtained to show how fast the precursors dissolved and reacted to produce the perovskite NCs. The PL emission peaks red-shifted with increasing sonication time. We found that the size of the perovskite NCs increased over time, eventually forming a plate-type morphology (see TEM images in the ESI,† Fig. S5).

In one possible growth model, the production of perovskite NCs follows the solubility of the precursor in toluene, *i.e.*, growth proceeds at a faster rate for precursors that are more soluble. We observed that the dissolution rates of MAX in toluene (in the presence of OAm) without PbX_2 followed the order MAI > MABr > MACl, while the solubilities of PbX_2 followed the order PbI_2 > $PbBr_2$ > $PbCl_2$. These orders are consistent with the relative ionic characteristics of the anions: the larger anions were less ionic, and the less ionic precursors dissolved better in the nonpolar solvent toluene. The slower growth rate of $CsPbBr_3$ compared to those of $FAPbBr_3$ and $MAPbBr_3$ was probably due to the lower solubility of CsBr because of its more ionic nature. We checked the relative solubilities of CsBr and FABr, and discovered that after 2 h CsBr remained undissolved, while more FABr than MABr was dissolved. We fitted the data using the exponential function $P(t) = 1 - e^{-kt}$, based on the pseudo-first-order reaction kinetics describing the dissolution rate of precursors in toluene. The data fitted this function well, and values of k = 0.029, 0.046, 0.16, 0.078, and 0.020 min^{-1} were obtained for $MAPbCl_3$, $MAPbBr_3$, $MAPbI_3$, $FAPbBr_3$, and $CsPbBr_3$, respectively.

We can tentatively conclude that the growth rate of the NCs was governed by a thermodynamic driving force based on the solubility of the precursors. Once the precursors were dissolved, the perovskite NCs were immediately crystallized in the poor solvent (toluene), and the long-chain organic ligand (OAm) acted as a soft template for their crystallization. Previous studies on the synthesis of perovskite NCs have used octylamine (or halide)

or OAm (or halide) ligands to produce the nanoscale crystals, based on the idea that the ligand binds to the perovskite with the alkyl chain extending outward, arresting crystal growth in that dimension.[12–20] However, the exact function of the large alkyl chain ligand on the nanocrystal formation is not still fully understood.

In the present work, OAm acted as a sufficiently protective ligand, stabilizing the surface of NCs and prohibiting aggregation into a large particle. We also tested shorter ligands such as octylamine and found that the NC size increased, resulting in a wide distribution in the range of 20–50 nm. Furthermore, a larger amount of OAm (*e.g.*, $APbX_3$: OAm = 1 : 6) reduces the size to 5 nm and gave a dot morphology, as evidenced by TEM and the blue-shift in the PL spectrum. These observations are summarized in the ESI,† Fig. S6. Since the PL intensities and stabilities of perovskite NCs were significantly reduced when the amount of OAm was increased, a 1 : 3 ratio of $APbX_3$: OAm was used.

The solubility of the precursors in the solvent has been found to be a key factor in the sonochemical synthesis of chalcogenide NCs.[29,32,33] Ultrasonic irradiation favors dissolution and thus accelerates the reaction, resulting in the precipitation of products. We observed that toluene mixed with OAm but did not dissolve the precursors well, with sonication increasing their degree of dissolution (see the ESI,† Fig. S7). Furthermore, toluene is an appropriate solvent in which the solubilities of the two precursors (AX and PbX_2) are similar to each other and are higher than that of the product, allowing for the precipitation of the perovskite NCs. We also tested other solvents such as dimethyl formamide (DMF), dimethyl sulfoxide (DMSO), and isopropyl alcohol (IPA). DMSO did not mix with OAm. All precursors were soluble in DMF without sonication, making it unsuitable for our synthetic mechanism. In the case of IPA, the solubility of PbX_2 was almost negligible compared to that of MAX, and thus the yield of perovskite NCs was much lower than when using toluene.

Fig. 3 shows the PL spectra of $APbX_3$ NCs in toluene on a normalized scale. The full widths at half maxima were narrow and had an average value of 25 nm (~100 meV). The photographs above the spectra show the fluorescent NCs under a UV lamp. Bright emission was observed over a wide wavelength range of 400–800 nm (3.1–1.5 eV). PL peaks appeared at 3.05 eV (407 nm) for $MAPbCl_3$, 3.18 eV (390 nm) for $CsPbCl_3$, and 3.00 eV (413 nm) for $FAPbCl_3$. The PL peaks of $MAPbBr_3$, $CsPbBr_3$, and $FAPbBr_3$ appeared at 2.33 eV (532 nm), 2.43 eV (510 nm), and 2.29 eV (541 nm), respectively, while those of $MAPbI_3$, $CsPbI_3$, and $FAPbI_3$ appeared at 1.64 eV (756 nm), 1.88 eV (660 nm), and 1.54 eV (805 nm), respectively. The band gaps were determined from the position of these band edge emission peaks.

The band gap (E_g) increased as the effective ionic radius of the A-site cation decreased, *i.e.*, as the ionic radius decreased in the order FA > MA > Cs, the E_g value followed the order $CsPbX_3$ > $MAPbX_3$ > $FAPbX_3$ for a given halide X. This trend is consistent with the band gaps of similar-sized NCs or bulk perovskites reported in previous works (see the ESI,† Table S1). The band gaps of the NCs were larger than those of their bulk phases by 0.05–0.15 eV. The Bohr radii of $MAPbBr_3$, $MAPbI_3$, $CsPbBr_3$, and $CsPbI_3$ have reported values of 2.0, 2.2, 3.5, and 6 nm, respectively.[34,35] When the thickness is less than the Bohr diameter, this could cause quantum size effects and consequently a blue shift in the PL peak. Therefore, the increase in E_g can be simply explained by quantum size effects. The quantum yields were measured as shown in Fig. S8 (ESI†).

We also synthesized a mixed halide series: $MAPbBr_{3-x}Cl_x$, $MAPbBr_{3-x}I_x$, $CsPbBr_{3-x}Cl_x$, and $CsPbBr_{3-x}I_x$. Fig. S9 (ESI†) shows their PL emission spectra on a normalized scale. The band gaps, determined from the position of the PL peak, are plotted as a function of x. The E_g of $APbBr_{3-x}Cl_x$ increased almost linearly with increasing x, with the observed linear dependence of E_g on x correlating well with previous studies.[16] The E_g of $CsPbX_3$ was always higher than that of $MAPbX_3$ for a given halide composition. The XRD patterns of the products showed perovskite phases with high purities (ESI,† Fig. S10). Thus, band gap tuning was achieved over a wide range by controlling the halide anion composition.

Photodetector devices were fabricated by spin-coating perovskite NC films (thickness = 3 μm) between two Au electrodes (on SiO_x substrates) separated by a gap of 2 μm. In these

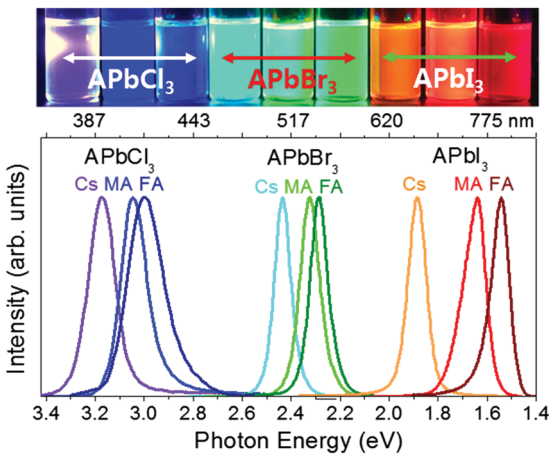

Fig. 3 PL spectra of composition-tuned $APbX_3$ perovskite NCs, where A = MA, Cs, or FA, and X = Cl, Br, or I. Photographs of the colloidal NCs under UV-lamp (Hg vapor lamp) irradiation are shown in the top row.

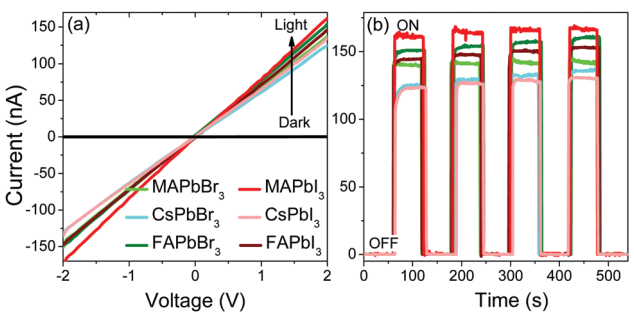

Fig. 4 (a) *I–V* characteristics of $APbBr_3$ and $APbI_3$ films, where A = MA, Cs, or FA, under 365 nm irradiation (60 mW cm^{-2}) and dark conditions. (b) *I–t* curves at a bias voltage of 2 V under chopper operation.

devices, 10 nm plate-type $APbBr_3$ and $APbI_3$ NCs were used, where A is MA, Cs, or FA. Fig. 4a shows the current–voltage (*I–V*) curves of the photodetector devices in the dark and under light irradiation. A 365 nm (3.4 eV) LED (60 mW cm^{-2}) was used as the light source. The *I–V* curves were almost linear within the measured voltage range (−2 to 2 V), indicating excellent ohmic contact. The dark current was ~1 pA. The current–time (*I–t*) curves at a bias voltage of 2 V were collected in real time through a series of on/off cycles (Fig. 4b). The current instantly increased when the device was illuminated and decreased when the device was switched off. The photocurrent (=ΔI) is defined as the increase in the current under illumination; the ΔI values were about 150 nA for all six types of $APbBr_3$ and $APbI_3$ NCs. We examined previously reported studies of photodetectors constructed using perovskites (see the ESI,† Table S2). To the best of our knowledge, no studies have reported comparisons of the compositions.

Time-resolved PL spectra were measured for the NCs in toluene and as 3 μm thick films (ESI,† Fig. S11). The decay curves were fitted with an exponential decay function (ESI,† Table S3). The decay times of the solutions followed the order FA > MA > Cs. However, the decay times of the films had similar values for all the NCs. Atomic force microscopy revealed that the roughness of the film was about 100 nm, irrespective of the film composition, probably because of the uniform sizes and shapes of the NCs (ESI,† Fig. S12). The NC film morphologies may have played a major role in the similar decay times. The photosensitivity correlates well with the PL emission decay time, and excited states with similar lifetimes could have resulted in similar photocurrent values. Time-resolved PL spectra and photocurrents were measured for the $MAPbBr_{3-x}Cl_x$, $MAPbBr_{3-x}I_x$, $CsPbBr_{3-x}Cl_x$, and $CsPbBr_{3-x}I_x$ NCs (ESI,† Table S4 and Fig. S13, S14). A similar composition dependence was observed for both the MA and Cs series. Among the mixed halides, I_2Br exhibited the longest PL decay time and the highest photocurrents, which is consistent with our previous work.[16]

In summary, we developed a novel route for synthesizing $APbX_3$ perovskite NCs with a wide range of compositions, where A = MA, Cs, or FA, and X = Cl, Br, or I. The NCs were synthesized by ultrasonic irradiation of AX, PbX_2, and OAm in toluene. We also synthesized a series of mixed halide NCs, including $MAPbBr_{3-x}Cl_x$, $MAPbBr_{3-x}I_x$, $CsPbBr_{3-x}Cl_x$, and $CsPbBr_{3-x}I_x$. The compositions of mixed halide NCs coincided with those of the precursors (PbX_2 and MAX). NCs with different compositions all exhibited uniform plate-type morphologies with an average size of 10 nm. Ultrasonic irradiation accelerated dissolution of the precursors in toluene, which determined the growth rate of the NCs. Band gap tuning over a wide range (1.54–3.18 eV) was achieved by controlling the composition of cations (MA, Cs, and FA) and halide anions. We fabricated photodetectors by spin coating the $APbBr_3$ and $APbI_3$ NCs between Au electrodes patterned on SiO_x substrates. The resulting devices displayed highly similar photosensitivities that correlated with the similar PL decay times of the NC films. The application of perovskite NCs is expected to be extended to lasers and LED devices.

This research was supported by a Korea University Grant. The HVEM (Daejeon) measurements were performed at the KBSI. The experiments at the PLS were partially supported by MOST and POSTECH.

Notes and references

1 W. S. Yang, J. H. Noh, N. J. Jeon, Y. C. Kim, S. Ryu, J. Seo and S. I. Seok, *Science*, 2015, **348**, 1234.
2 S. D. Stranks and H. J. Snaith, *Nat. Nanotechnol.*, 2015, **10**, 391.
3 P. Umari, E. Mosconi and F. D. Angelis, *Sci. Rep.*, 2014, **4**, 4467.
4 A. Kojima, M. Ikegami, K. Teshima and T. Miyasaka, *Chem. Lett.*, 2012, **41**, 397.
5 C. Wehrenfennig, G. E. Eperon, M. B. Johnston, H. J. Snaith and L. M. Herz, *Adv. Mater.*, 2014, **26**, 1584.
6 V. D'Innocenzo, G. Grancini, M. J. P. Alcocer, A. R. S. Kandada, S. D. Stranks, M. M. Lee, G. Lanzani, H. J. Snaith and A. Petrozza, *Nat. Commun.*, 2014, **5**, 3586.
7 S. D. Stranks, G. E. Eperon, G. Grancini, C. Menelaou, M. J. P. Alcocer, T. Leijtens, L. M. Herz, A. Petrozza and H. J. Snaith, *Science*, 2013, **342**, 341.
8 Q. Dong, Y. Fang, Y. Shao, P. Mulligan, J. Qiu, L. Cao and J. Huang, *Science*, 2015, **347**, 967.
9 J. Burschka, N. Pellet, S. J. Moon, R. Humphry-Baker, P. Gao, M. K. Nazeeruddin and M. Grätzel, *Nature*, 2013, **499**, 316.
10 J. H. Noh, S. H. Im, J. H. Heo, T. N. Mandal and S. I. Seok, *Nano Lett.*, 2013, **13**, 1764.
11 J.-H. Im, I.-H. Jang, N. Pellet, M. Grätzel and N.-G. Park, *Nat. Nanotechnol.*, 2014, **9**, 927.
12 L. C. Schmidt, A. Pertegás, S. González-Carrero, O. Malinkiewicz, S. Agouram, G. M. Espallargas, H. J. Bolink, R. E. Galian and J. Pérez-Prieto, *J. Am. Chem. Soc.*, 2014, **136**, 850.
13 F. Zhang, H. Zhong, C. Chen, X.-G. Wu, X. Hu, H. Huang, J. Han, B. Zou and Y. Dong, *ACS Nano*, 2015, **9**, 4533.
14 D. Zhang, S. W. Eaton, Y. Yu, L. Dou and P. Yang, *J. Am. Chem. Soc.*, 2015, **137**, 9230.
15 B. Luo, Y.-C. Pu, Y. Yang, S. A. Lindley, G. Abdelmageed, H. Ashry, Y. Li, X. Li and J. Z. Zhang, *J. Phys. Chem. C*, 2015, **119**, 26672.
16 D. M. Jang, K. Park, D. H. Kim, J. Park, F. Shojaei, H. S. Kang, J.-P. Ahn, J. W. Lee and J. K. Song, *Nano Lett.*, 2015, **15**, 5191.
17 G. Nedelcu, L. Protesescu, S. Yakunin, M. I. Bodnarchuk, M. J. Grotevent and M. V. Kovalenko, *Nano Lett.*, 2015, **15**, 5635.
18 Q. A. Akkerman, V. D'Innocenzo, S. Accornero, A. Scarpellini, A. Petrozza, M. Prato and L. Manna, *J. Am. Chem. Soc.*, 2015, **137**, 10276.
19 J. Shamsi, Z. Dang, P. Bianchini, C. Canale, F. Di Stasio, R. Brescia, M. Prato and L. Manna, *J. Am. Chem. Soc.*, 2016, **138**, 7240.
20 A. Pan, B. He, X. Fan, Z. Liu, J. J. Urban, A. P. Alivisatos, L. He and Y. Liu, *ACS Nano*, 2016, **10**, 7943.

21 J. Song, J. Li, X. Li, L. Xu, Y. Dong and H. Zeng, *Adv. Mater.*, 2015, **27**, 7162.
22 Y. Ling, Z. Yuan, Y. Tian, X. Wang, J. C. Wang, Y. Xin, K. Hanson, B. Ma and H. Gao, *Adv. Mater.*, 2016, **28**, 305.
23 M. Cha, P. Da, J. Wang, W. Wang, Z. Chen, F. Xiu, G. Zheng and Z. S. Wang, *J. Am. Chem. Soc.*, 2016, **138**, 8581.
24 S. Yakunin, L. Protesescu, F. Krieg, M. I. Bodnarchuk, G. Nedelcu, M. Humer, G. D. Luca, M. Fiebig, W. Heiss and M. V. Kovalenko, *Nat. Commun.*, 2015, **6**, 8056.
25 Y. Wang, X. Li, J. Song, L. Xiao, H. Zeng and H. Sun, *Adv. Mater.*, 2015, **27**, 7101.
26 P. Ramasamy, D. H. Lim, B. Kim, S. H. Lee, M. S. Lee and J. S. Lee, *Chem. Commun.*, 2016, **52**, 2067.
27 Y. Shirasaki, G. J. Supran, M. G. Bawendi and V. Bulović, *Nat. Photonics*, 2013, **7**, 13.
28 W. Rehman, R. L. Milot, G. E. Eperon, C. Wehrenfennig, J. L. Boland, H. J. Snaith, M. B. Johnston and L. M. Herz, *Adv. Mater.*, 2015, **27**, 7938.
29 J. H. Bang and K. S. Suslick, *Adv. Mater.*, 2010, **22**, 1039.
30 Y. Kesari and A. Athawale, *Mater. Lett.*, 2015, **159**, 87.
31 V. B. Kumar, L. Gouda, Z. Porat and A. Gedanken, *Ultrason. Sonochem.*, 2016, **32**, 54.
32 Q. Li, Y. Ding, M. Shao, J. Wu and Y. Qian, *Mater. Res. Bull.*, 2003, **38**, 539.
33 B. T. Mayers, K. Liu, D. Sunderland and Y. Xia, *Chem. Mater.*, 2003, **15**, 3852.
34 K. Tanaka, T. Takahashi, T. Ban, T. Kondo, K. Uchida and N. Miura, *Solid State Commun.*, 2003, **127**, 619.
35 L. Protesescu, S. Yakunin, M. I. Bodnarchuk, F. Krieg, R. Caputo, C. H. Hendon, R. X. Yang, A. Walsh and M. V. Kovalenko, *Nano Lett.*, 2015, **15**, 3692.